ROYAL SOCIETY OF CHEMISTRY

PCCP

Actinyl cation-cation interactions in the gas phase: An accurate thermochemical study

Journal:	*Physical Chemistry Chemical Physics*
Manuscript ID	CP-ART-02-2019-000760.R1
Article Type:	Paper
Date Submitted by the Author:	20-Mar-2019
Complete List of Authors:	Feng, Rulin; Washington State University, Department of Chemistry Glendening, Eric; Indiana State University, Department of Chemistry Peterson, Kirk; Washington State University, Department of Chemistry;

SCHOLARONE™
Manuscripts

Actinyl cation-cation interactions in the gas phase: An accurate thermochemical study

Rulin Feng[†], Eric D. Glendening[‡], and Kirk A. Peterson[*,†]

[†]Department of Chemistry, Washington State University, Pullman, Washington 99164-4630

[‡]Department of Chemistry, Indiana State University, Terre Haute, Indiana 47809

Abstract

Gas phase actinyl cation-cation interactions (CCIs) were studied by an accurate composite coupled cluster thermochemical approach for the first time. A number of CCI dimers were constructed from the monomers UO_2^{2+}, UO_2^+, NpO_2^{2+}, NpO_2^+, PuO_2^+, and AmO_2^+. All CCI dimers studied were calculated to be thermodynamically unstable, with dissociation energies ranging from -60 to -90 kcal/mol, but in many cases kinetic stability was indicated by calculated local minima with well depths as large as ~15 kcal/mol. Most of the dimers studied involved a T-shaped geometry, although one side-on dimer, $(UO_2^+)_2$, was included since it was amenable to coupled cluster methods. In the T-shaped isomers the most stable dimers were calculated to arise when the oxo-group of an An(V) actinyl cation was oriented towards the metal center of an An(VI) actinyl cation. For both mixed-valent An(VI)/An(V) and mono-valent An(V) dimers, the stability as estimated from the depth of the calculated local minimum decreased in the donor series U(V)>Np(V)>Pu(V)>Am(V). These trends correlate well with experimental trends in condensed phase CCIs. A rationale for the bonding in CCIs was investigated by carrying out charge transfer analyses using the natural bond orbital (NBO) method. Augmenting the usual Lewis acid-base explanation, CCIs are the direct result of a competition between charge transfer stabilization, which can be as much as 0.11e or 30.7 kcal/mol at equilibrium, and Coulombic repulsive destabilization.

---

[*] E-mail: kipeters@wsu.edu

I. INTRODUCTION

Particular bonding types between cations have been observed in solid-state physics for many years. Goodenough and co-workers first proposed the concept of cation-cation interactions between transition metal oxides more than 50 years ago.[1] It was proposed to account for the magnetism of certain materials by providing an electron exchange pathway between two metal cations.[2] Soon after that, Sullivan et al.[3] observed the complexation of actinyl cations (AnO_2^{n+}) in a mixture of $Np(V)O_2^+$ and $U(VI)O_2^{2+}$ cations in various concentrations of aqueous perchloric acid media. This is the first recorded cation-cation interaction (CCI) involving elements from the actinide series. The complex was later shown to be $[UO_2^{2+} \bullet NpO_2^+]$, with an oxygen end of the neptunyl cation directed at the metal center of the uranyl, forming a T-shaped dimer structure.[4-6] After the characterization of many other species containing these types of coordination in different phases[7-9], the term "cation-cation interaction" has been primarily referred to as an oligomerization interaction involving actinyl cations. CCIs have been given special attention not only because of the interest in understanding their novel bonding type, but also the various possibilities of elucidating current actinide crystalline material structure, actinide solution chemistry, or inspiring possible new materials and cleaner nuclear fuel processing.[8, 10] While several types of actinyl coordination have been observed in the solid state,[8] two distinct dimerization configurations as shown in Figure 1 can be extracted. When an oxo group of one actinyl is directed towards the metal center of another actinyl, a T-shaped CCI dimer results. This has previously been interpreted as a typical Lewis acid-base interaction.[11] On the other hand, a so-called side-on dimer results when the actinyls are oriented in a slipped-parallel arrangement so that each monomer can act as both an acceptor and donor. The latter is rare, but Vlaisavljevich and co-workers[12] recently reported the synthesis and characterization of a crystalline sheet structure that contained $[NpO_2^+ \bullet NpO_2^+]$ side-on configurations.

In the past few years, researchers have continued discovering new features and structures of actinide CCIs. The stability of actinyl(V) ions (AnO_2^+) in aqueous solution is generally dictated by their disproportionation reactions[13],

$$2AnO_2^+ + 4H^+ \rightarrow An^{4+} + AnO_2^{2+} + 2H_2O$$
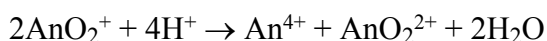
The reaction involving U(V) is known to be very rapid over most pH ranges, while Np(V) is the dominant oxidation state of Np in solution. Steele and Taylor[14] have proposed the participation

of CCI dimers in an inner-sphere disproportionation reaction mechanism for both U(V) and Pu(V) actinyl cations using Hartree-Fock (HF) and density functional theory (DFT) approaches. Several groups have successfully synthesized and characterized many different sodium neptunyl(V, VI) crystals based on distinct CCI network patterns,[15-21] while other studies have reported the successful synthesis and characterization of uranyl(V, VI) complexes connected by CCI complexes, among which uranyl(VI) CCIs only account for ~2% of uranyl(VI) compounds.[22-24] It has also been suggested that CCIs between neptunyl(V) cationic units provide potential superexchange pathways that enhance magnetic interactions in the oligomerization or crystallization process.[2] A review by Krot and Grigoviev[8] of the previous experimental studies involving crystalline compounds showed that there are many more CCIs in Np(V) containing compounds than those containing Np(VI) or U(VI). It was also pointed out that the stability of An(V) cation-cation complexes with a donating oxo group decreases with increasing atomic number $UO_2^+ > NpO_2^+ > PuO_2^+ > AmO_2^+$; for doubly charged actinyls as coordinating centers, the stability also follows the same trend $UO_2^{2+} > NpO_2^{2+} > PuO_2^{2+} > AmO_2^{2+}$. From a coordinating environment perspective, they also concluded that the incorporation of a large number of water molecules into the crystal structure would weaken the CCI, which can also be seen upon transition of CCI crystals to those in aqueous solution, where the stability of the CCI complexes are generally much weaker in the latter. Given the relatively large dielectric constant of water, however, this should lead to a stronger CCI if coulombic forces were the key contributor to the CCI strength. Instead, the present work indicates that the inner-sphere coordination of an oxo-group to another actinyl is the main factor, i.e., the charge transfer from the oxo group on one actinyl to the metal center on the other actinyl plays the decisive role.

In the gas phase, the properties of multiply charged complexes have been extensively studied by both experiment and theory (see Ref. 25 and references therein). Such a complex is thermodynamically stable if the energy of the complex lies below that of the lowest separated asymptotes. For the dication case, e.g., AB^{2+}, the two relevant asymptotes would be $A^{2+} + B$ and $A^+ + B^+$. Since the potential curve of the former is attractive, AB^{2+} will be thermodynamically stable if the ionization potential (IP) of A^+ is less than that of B or if the bond strength of AB^{2+} is sufficiently large to make up for a somewhat too large IP(A^+). As the IP of A^+ increases, the AB^{2+} minimum can rise above the $A^+ + B^+$ asymptote, and the complex will be metastable with respect to dissociation (and eventually completely unstable). The resulting well depth of a

metastable AB^{2+} complex is governed by the barrier arising from the crossing of the repulsive A^+ + B^+ potential with the attractive ion-neutral potential. The charge separation reaction can be very exothermic, i.e., a Coulomb explosion, but the metastable complex can have extensive kinetic stability if the barrier is sufficiently high. As will be demonstrated in this work, all of the actinyl cation-cation complexes are thermodynamically unstable in the gas phase, but nearly all are predicted to possess kinetic stability as evidenced by their calculated barriers and associated well depths.

Despite the considerable experimental work that have been carried out to synthesize materials or solutions utilizing CCIs, fundamental knowledge that helps rationalize the formation of different CCI oligomers is still very limited.   Previous theoretical investigations have included only a few studies, since ab initio calculations involving actinyl-actinyl complexes are particularly demanding because of strong relativistic effects, large numbers of electrons, and closely spaced low-lying exited states, . Using DFT with a polarized triple-zeta (TZ2P) basis set and the ZORA relativistic Hamiltonian, McKee and Swart[11] carried out a thermochemical study for $Np(V)O_2^{+/2+}$ and $U(VI)O_2^{+/2+}$ dimerizations for both gas and aqueous phases. The solvation effects were modeled using COSMO. Their main conclusion was that actinyl-actinyl CCI complexes are thermodynamically unstable in the gas phase, while in aqueous phase, solvation effects stabilized most of the CCI complexes.   The uranyl-uranyl dimer, however, (total charge of +4) was calculated to be unstable even with solvation included. In agreement with the observations in crystalline materials, they found the stable (local minima) structures adopted T-shape configutrations. More recently, Vlaisavljevich et al.[12] carried out a high-level ab initio study of $Np(V)O_2^+$ dimers using spin-orbit complete active space 2nd-order perturbation theory (SO-CASPT2) with TZ atomic natural orbital (ANO) basis sets and the 2nd-order Douglas-Kroll-Hess (DKH2) relativistic Hamiltonian.   They compared the $[NpO_2^+ \cdot NpO_2^+]$ side-on dimer to its T-shaped isomer via a scan of its potential energy surface connecting the two, and concluded that the side-on dimer was more stable by about 6 kcal/mol. They also demonstrated that the perturbational treatment of spin-orbit coupling made little change to the energy landscape of these dimers. Last, a DFT study using scalar relativistic, small-core effective core potentials (ECPs), as well as all-electron ZORA calculations, was recently reported by Tecmer et al.[26] for $U(V/VI)O_2^{1+/2+}$ dimers.   They investigated both side-on and T-shaped configurations with various spin couplings, including solvation effects in aqueous media modeled by COSMO,

and included calculations of their vibrational and UV-Vis spectra. Inspection of their results suggested that a greater number of unpaired electrons weakens the dimer complexes, and the T-shaped dimers are more stable than the side-on ones for uranyl CCI complexes in solution. They also demonstrated that the singlet, anti-ferromagnetic coupled state of the U(V)-U(V) dimer was much less stable than its high spin triplet state. Even with these previous theoretical studies, it is still not completely clear what physical effects govern the stability of given CCI complex. Thus molecular structures containing CCIs still cannot be designed a priori due to lack of understanding of the nature of these interactions.

The goal of the present study is to provide such a fundamental understanding by choosing a wider range of CCI dimers than previously studied, as well carrying out these studies with much higher levels of electron correlation, basis set sizes, and recovery of spin-orbit coupling and relativistic effects. The present work is restricted to the gas phase, but it is fully expected that the binding and structural trends will be consistent with those in condensed media. To this end, T-shaped actinyl-actinyl CCI dimers $[UO_2^{2+} \bullet UO_2^+]$, $[UO_2^+ \bullet UO_2^+]$, $[UO_2^{2+} \bullet NpO_2^+]$, $[NpO_2^{2+} \bullet UO_2^+]$, $[NpO_2^{2+} \bullet NpO_2^+]$, $[NpO_2^+ \bullet NpO_2^+]$, $[PuO_2^+ \bullet PuO_2^+]$, and $[AmO_2^+ \bullet AmO_2^+]$ have been investigated using coupled cluster theory with the 3rd-order Douglas-Kroll-Hess (DKH3) scalar relativistic Hamiltonian together with all electron correlation consistent basis sets. One side-on dimer, $[UO_2^+ \bullet UO_2^+]$, was also studied to understand the relative stability between T-shaped and side-on dimers. Detailed natural bond orbital (NBO) analyses have also been performed to elucidate the underlying origin of stable CCIs and to explore new explanations for their occurrence.

II. COMPUTATIONAL DETAILS

A. Systems studied

While actinyl-actinyl dimers are known to be thermodynamically unstable with respect to dissociation to their respective monomers in the gas phase, they do possess stable local minima. In the present work, several actinyl-actinyl dimer combinations were investigated by carrying out geometry optimizations at the restricted open-shell Hartree-Fock, unrestricted coupled cluster singles and doubles with perturbative triples, ROHF-UCCSD(T), level of theory[27-29] using the DKH3 scalar relativistic Hamiltonian[30-32] with valence triple-zeta (VTZ) quality basis sets, cc-

pVTZ-DK3 on the actinides[33] and aug-cc-pVTZ-DK on oxygen.[34-36] All valence electrons were correlated, i.e., 6s through 7s on the actinides and 2s, 2p on oxygen, and only high spin states, which also correspond to the ground electronic states for all the monomer species, were considered since only these are amenable to single reference coupled cluster theory. This level of theory will be referred to as CCSD(T)/VTZ throughout this work. In the initial survey, the An-O bonds were fixed to their monomer values optimized at the same level of theory, see Table I, with the O-An-O bond lengths constrained to be linear. It should be noted that it was shown previously by Infante et al.[37] that the wavefunctions of these monomers are generally dominated by their Hartree-Fock configurations, with the worst case being AmO_2^+, where the leading configuration still had a weight of 0.85. As shown in Table II, a total of 34 T-shaped dimers were investigated, which involved 11 homodimers and 23 heterodimers. Of these 34 systems, only a total of 10 were found to have stable (local) minima. Eight of these were then fully optimized at the CCSD(T)/VTZ level of theory and subjected to further detailed thermochemical study as described below. A total of 9 side-on dimers were also investigated, the homodimers $(UO_2^+)(UO_2^+)$, $(NpO_2^+)(NpO_2^+)$, $(PuO_2^+)(PuO_2^+)$, and $(AmO_2^+)(AmO_2^+)$ and heterodimer species $(UO_2^+)(NpO_2^+)$, $(UO_2^{2+})(UO_2^+)$, $(UO_2^{2+})(NpO_2^+)$, $(NpO_2^{2+})(UO_2^+)$, and $(NpO_2^{2+})(NpO_2^+)$. Nearly all of these side-on dimers were too multireference to reliably use the CCSD(T) method, except for $UO_2^+UO_2^+$ and the +3 heterodimers $UO_2^{2+}UO_2^+$ and $NpO_2^{2+}UO_2^+$. However in the latter two cases, these dimers were unstable with respect to either dissociation or rearrangement to the T-shaped geometries. Hence only the $(UO_2^+)(UO_2^+)$ side-on dimer was subjected to further optimization and analysis.

From Table II, it can be observed that a metastable T-shaped dimer is formed when and only when the donor monomer has a +1 charge, while the charge of the acceptor can be +1 or +2. A +3 acceptor doesn't appear to result in a metastable dimer, but it is difficult to definitively rule them out since the interaction with a +1 actinyl donor leads to very strong charge transfer and large multireference effects that prevent the reliable use of single determinant methods like CCSD(T). While the outcomes for side-on dimers are not shown in Table II, they have a much simpler behavior – for all tested cases, only +2 charged homodimers, i.e., (+1)(+1), were found to form metastable, side-on dimers.

In addition to fully optimizing the separated monomers and their dimer complexes, approximate transition state geometries were also optimized for the eight stable T-shaped dimers.

In these calculations the complexes were constrained to have C_{2v} symmetry with monomer geometries fixed to their optimal values in the dimer complexes. These latter bond lengths were chosen since the barrier occurs very late in the reaction coordinate. Hence the transition state geometry was defined by just the distance beween the metal atom of the acceptor and the nearest oxo group of the donor, $R_b{}^{CCI}$.

B. Composite thermochemistry

For the isolated monomers, the stable T-shaped dimers described above, their approximate transition states, as well as the $UO_2{}^+$ side-on homodimer, the Feller-Peterson-Dixon (FPD) composite thermochemistry approach[38-40] was applied at the TZ optimized geometries via

$$E_{FPD} = E_{VQZ} + \Delta E_{CBS} + \Delta SO + \Delta Gaunt \; (+ \; \Delta E_{ZPE}) \tag{1}$$

In Eq. (1), E_{VQZ} is the frozen-core ROHF-UCCSD(T) (also referred to as R/UCCSD(T)) energy calculated with cc-pVQZ-DK3 basis set for the actinides and aug-cc-pVQZ-DK for oxygen in conjunction with the DKH3 scalar relativistic Hamiltonian. The second term, $\Delta E_{CBS,}$ is the difference between the latter VQZ result and the energy extrapolated to the complete basis set (CBS) limit using the TZ and QZ basis sets. In this work the Hartree-Fock (HF) energy and CCSD(T) correlation energy were extrapolated separately. The HF CBS limit was calculated utilizing the Karton-Martin formula[41] with $n=3$ and 4

$$E_n = E_{CBS} + A(n+1)e^{-6.57\sqrt{n}} \tag{2}$$

The correlation energy CBS limit was obtained using[42, 43]

$$E_n = E_{CBS} + \frac{B}{\left(n + \frac{1}{2}\right)^4} \tag{3}$$

also with $n=3$ and 4.

The third and fourth terms, ΔSO and $\Delta Gaunt$, are both predominately contributions of spin-orbit (SO) coupling, the first from the Dirac-Coulomb Hamiltonian and the second from inclusion of the Gaunt operator.   Calculation of both contributions utilized uncontracted cc-pVDZ-DK3 basis sets for the actinides and aug-cc-pVDZ-DK basis sets for oxygen. The average-of-configuration (AOC) Dirac-Hartree-Fock (DHF) method was employed followed by a complete open-shell configuration interaction (COSCI) calculation[44] to resolve the ground state eigenvalues. In each case only the small number of open shell electrons were distributed among

the spinors arising from the 5f electrons.   The ΔSO value was calculated as the difference between the 4-component Dirac-Coulomb result and the energy from an analogous calculation using Dyall's spin-free Hamiltonian.[45] The ΔGaunt term was obtained in the same manner except the difference was between SO calculations with or without the two-electron Gaunt term in the Hamiltonian. In all of these calculations a finite nucleus model was used.[46]

For the calculation of CCI dissociation energies, an additional term accounting for the vibrational zero-point energy, ΔE_{ZPE}, was added to the total energy.   These were calculated at the harmonic level using the DKH3 R/UCCSD(T) method with cc-pVDZ-DK3 (An) and aug-cc-pVDZ-DK (O) basis sets.   The hessian was calculated using double numerical differentiation of energies.

The MOLPRO program suite[47, 48] was utilized for the majority of the present calculations, however harmonic frequencies were calculated using the CFOUR[49] package with the individual displacement energies obtained from MOLPRO. All spin-orbit calculations were carried out using the DIRAC[50] program.

C. Natural bond orbital analysis

Wavefunction analysis was carried out at the HF level using NBO methods.[51]   These methods calculate a "natural Lewis structure" (NLS) of localized one- and two-center orbitals that describes as much of the total electron distribution as possible.   Electron density that is missing from the NLS resides in so-called non-Lewis orbitals, principally in formally unoccupied two-center functions (antibonds).   Second-order perturbative analysis of the NBO Fock matrix identifies the leading electron donor-acceptor delocalizations that account for the missing density of the NLS.   For this study, the perturbative treatment of intermolecular (charge transfer) delocalizations for the actinyl dimers is of particular interest.

An initial assessment of the actinyl monomers revealed $6p_z$ natural atomic orbitals (NAOs) on the An centers that lack as much as a tenth of an electron because they participate in valence bonding interactions.   For example, the U $6p_z$ of UO_2^{2+} has an occupancy of 1.915 electrons, significantly less than the 1.99+ electrons of the more core-like 6s and $6p_x$/$6p_y$ orbitals.   Thus, we chose to modify the default NAO core/valence partitioning to treat the 6s and 6p orbitals as valence functions for all calculations reported here.   Although the uranyl $6p_z$ loses more electron density when treated as valence (its occupancy decreases from 1.915 to 1.645 electrons

now that the orbital can more freely participate in bonding), the resulting NLS better describes the total electron distribution.   That is, the NLS for uranyl with the modified core/valence partitioning accounts for all but 0.168 electrons of the ion's 106 electrons (99.84% of 106), whereas the standard partitioning yields an NLS that describes all but 0.370 electrons (99.65% of 106).   The lower "non-Lewis density" (0.168 vs. 0.370) of the NLS warrants the use of the non-standard core/valence partitioning for our analysis here.

All NBO calculations were performed using the MOLPRO interface to NBO 7.0. [52]

III. RESULTS AND DISCUSSION

A. Dissociation energies and cation-cation interaction barriers

In the present work a total of seven T-shaped CCI dimers were chosen to apply the FPD composite approach for dissociation energies (to the separated monomers) and CCI barrier heights (relative to the local CCI minima). These were $(UO_2^{2+})(UO_2^+)$, $(UO_2^{2+})(NpO_2^+)$, $(UO_2^+)(UO_2^+)$, $(NpO_2^{2+})(UO_2^+)$, $(NpO_2^+)(NpO_2^+)$, $(PuO_2^+)(PuO_2^+)$, and $(AmO_2^+)(AmO_2^+)$. The side-on dimer of $(UO_2^+)(UO_2^+)$ was also included. The resulting dissociation energies, together with their FPD components from Eq (1), are shown in Table III. Clearly, in all cases the CCI complexes are very thermodynamically unstable with respect to dissociation into their respective monomer cations in the gas phase. In regards to the effects of spin-orbit coupling, both spin-same-orbit (ΔSO) and the Gaunt contribution ($\Delta Gaunt$), these tend to uniformly make the complexes less stable by a total of about 1–5 kcal/mol. The zero-point vibrational effects, ΔZPE, are relatively small, since these weak interactions do not invoke significant vibrational changes. It can be seen from Table III that the dissociation energy is about 30-40 kcal/mol more negative when the charge of the acceptor is +2 compared to +1 due to the greater repulsive forces. In addition, within the (+2)(+1) cases, the dimer with the larger number of openshell electrons is more thermodynamically unstable; the contribution per openshell electron is about -5 kcal/mol for the acceptor and about -7 kcal/mol for the donor. In the (+1)(+1) cases, the thermodynamic stability also decreases from An=U to Am, but the $(NpO_2^+)(NpO_2^+)$ dimer is much less stable. The side-on isomer of $(UO_2^+)(UO_2^+)$ is calculated to be thermodynamically more stable than its T-shaped isomer by nearly 10 kcal/mol. The apparent anomaly in the Np(V) dissociation energy can be partially understood by considering the difference in energy between the two dissociation asymptotes as discussed in the Introduction, i.e., $AnO_2^{2+} + AnO_2$ and $AnO_2^+ + AnO_2^+$. To a

certain extent, the dissociation energy of the CCI complex is constrained by the difference in energy of these two asympototes, i.e., IP(AnO$_2^+$) – IP(AnO$_2$). As this separation becomes larger, the crossing point will presumably occur at higher energies, yielding a larger negative dissociation energy. From the known ionization potentials of the actinide dioxides,[53] albeit some with considerable experimental uncertainties, the An=Np case is predicted to be larger than the other actinides studied here [in kcal/mol: 195 (U), 203 (Np), 187 (Pu), 196 (Am)], which would lead to a more negative dissociation energy.

Although these T-shaped actinyl CCI dimers have been shown to be thermodynamically unstable, they obviously have local minima that imply at least some kinetic stability in the gas phase. It should be noted that previous solvation model calculations by both McKee and Swart on Np(V)/U(VI) dimers,[11] as well as Tecmer et al. on U(V)/U(VI) dimers,[26] suggest that all of the present dimers will be stable with respect to dissociation in aqueous solutions. Hence aqueous solvent is predicted to preferentially stablize the dimers compared to the separated monomers. In this work the gas phase metastability has been studied for the first time for the T-shaped dimers by following a reaction path defined by the An–O distance with the constraints of C$_{2v}$ symmetry using linear monomers with fixed bond lengths. A representative CCI curve is shown in Figure 2 for (NpO$_2^{2+}$)(UO$_2^+$). Dissociation curves for the heteroactinyl dimers (UO$_2^{2+}$)(UO$_2^+$), (UO$_2^{2+}$)(NpO$_2^+$), (NpO$_2^{2+}$)(NpO$_2^+$), and (NpO$_2^{2+}$)(UO$_2^+$) are given in Figure 3, while those for the homoactinyl dimers are in Figure 4. For the cases of doubly-charged acceptors shown in Figure 3, the depths of the wells are mostly determined by the identity of the donor actinyl, and more open-shell electrons on the donor reduce the barrier height and subsequent (meta)stability of the CCI dimer. Moreover, in Figure 4 a systematic decrease of the barrier height, and concomitant decrease in the magnitude of the well depth, is also observed for the homoactinyl dimers with an increasing number of open-shell electrons. This is in accordance with the trend found by Krot and Grigoriev from condensed-phase experiments[8], i.e., if the CC complex has more electrons, then the stability decreases. The results of the FPD composite approach for the CCI barrier heights are given in Table IV. The spin-orbit contributions are much smaller than those from dissociation to monomer units, with the largest ΔSO contribution calculated for (UO$_2^{2+}$)(UO$_2^+$) with a value of +1.10 kcal/mol. The inclusion of the Gaunt term, however, brings the total effect from SO coupling down to just +0.38 kcal/mol. The sum of ΔSO and ΔGaunt only amounts to a few tenths of a kcal/mol for nearly all cases, except for (UO$_2^+$)(UO$_2^+$) where it is calculated to be –1.12 kcal/mol. In general the barrier heights from the

mixed valent dimers, An(VI)•An(V), are generally much larger (implying greater kinetic stability) than the An(V)•An(V) cases, which is not unexpected since the former are most commonly observed in experiments[8]. The dimers with the deeper local minima also have shorter R_e^{CCI} values but longer R_b^{CCI}. The barrier almost disappears for $AmO_2^+AmO_2^+$, with a barrier height of only 0.02 kcal/mol at the spin-free level. However when spin-orbit coupling is included, the barrier completely disappears to a value of -0.15 kcal/mol, i.e., this CC complex is unstable with respect to dissociation.

From Tables III and IV it is clear that the mixed valent species, while being much less thermodynamically stable, form more strongly bound metastable CCI complexes compared to the +2 homovalent dimers, but it is not clear how that translates to which species are more prevalent in condensed phases, since the (+2)(+1) heterodimers need to overcome much stronger repulsive forces (note the dissociation energies of Table III) at long range compared to the (+1)(+1) complexes. Experimentally in condensed phase the (+1)(+1) CCIs are certainly more prevalent.

In regards to the equilibrium CCI dimer structures shown in Table IV, the (+2)(+1) heterodimers have R_e^{CCI} bond distances of about 2.45 Å, which are about 0.3 Å shorter than the average bond lengths of the (+1)(+1) homodimers. The acceptor species in the former cases are all nearly linear, while those of the homodimers are bent from linearity by as much as ~6°. In both cases the bond lengths of the acceptor moeties are nearly unchanged from the separated monomers, however significant changes are calculated in the donor structures; namely Δr_1 lengthens by as much as 0.15 Å and Δr_2 shortens by up to 0.03 Å. The changes for the (+2)(+1) dimers are nearly twice as large as those for the (+1)(+1) cases. In the $(UO_2^+)(UO_2^+)$ side-on dimer (not shown in Table IV), R_e^{CCI} is 2.402 Å and the value of r_{d1} lengthens by 0.12 Å (see Fig. 1), which is only slightly less than that of the T-shaped (+2)(+1) dimers. Compared to reported U and Np CCI distances in condensed phases,[8] the latter show considerable variability depending on the associated ligands, but the average is very simlar for the U(VI) cases and about 0.3 Å shorter for Np(V) compared to the current gas phase results.

In comparison to previous calculations of these species in the gas phase, some of the present CCSD(T) results can be compared to the BPW91/TZ2P DFT results of McKee and Swart.[11] Their result for R_e^{CCI} of the $(UO_2^{2+})(NpO_2^+)$ dimer, 2.465 Å, is nearly identical to the present optimized coupled cluster value of 2.469 Å. However their analogous result for the

$(NpO_2^+)(NpO_2^+)$ dimer, 2.621 Å, is much shorter than the CCSD(T) value of 2.725 Å. Likewise, their DFT dissociation energy calculated for the $(UO_2^{2+})(NpO_2^+)$ dimer is within about 2 kcal/mol of the present FPD result, while the DFT result for $(NpO_2^+)(NpO_2^+)$ is more strongly bound by 9 kcal/mol. The changes in r_{d1} upon complexation for both clusters followed similar trends between the two dimers.

To this point, the stability of a given CCI actinyl dimer has been shown to be most strongly governed by (i) the identity of the donor actinyl; those involving An(V) with the smallest number of open-shell electrons leads to the strongest interactions and (ii) an acceptor An(VI) actinyl leads to more strongly bound CCIs. These results can be partially explained by the usual rationale of CCI bonding in that they are primarily Lewis acid-base interactions. The fact that An(VI) actinyls are obviously better Lewis acids than An(V) species matches well with the second of these trends. A recent review[54] notes that Np(V) will be a more effective donor than U(VI) since the $5f^2$ open-shell configuration of Np(V) will increase the electrostatic repulsions between the actinide and its oxo units, thus increasing its Lewis basicity compared to U(VI) which has no open-shell electrons. This latter explanation, however, does not help explain the well depth trend of this work when comparing dimers containing U(V) to Am(V), where increasing the number of open-shell 5f electrons *decreases* the depth of the local minimum and hence the dimer's stability.

B. Natural bond orbital analysis

We now turn attention to NBO analysis of cation-cation interactions in the actinyl dimers by first considering the bonding patterns of the monomers, as detailed in Table V.   For each monomer the Lewis structure reveals the hexavalent character of the An center, including a pair of An-O triple bonds, a lone pair on each O center, and unpaired electrons, if any, localized in An 5f orbitals.   The unpaired electrons, which are not described in Table V, reside in 5f NAOs of the same symmetries as listed in the configurations of Table I.   Each O has a lone pair of predominantly 2s character (by 84-89%), allowing the 2p orbitals to participate in triple bonds with An.   The σ_{AnO} bonds consist of an An hybrid of approximate pd^3f^2 character (one-sixth 6p, one-half 6d, and one-third 5f) and an O hybrid is that is largely $2p_z$ (86-89%).   The π_{AnO} bonds consist of a df hybrid (one-half 6d and one-half 5f) on An and pure 2p on O.   The π

bonds (~50-60% ionic character) are somewhat more polarized toward the more electronegative O centers than the σ bonds (~40% ionic).   The σ bonds are particularly interesting here because the An $6p_z$, which is nominally considered a core orbital, contributes significantly to these valence bonding functions.   The two core-like electrons that would have resided in the $6p_z$ instead occupy a core-like hybrid of roughly p^2f (two-thirds 6p and one-third 5f) character. The latter accounts for two-thirds of the $6p_z$ character with the remainder in the two sigma bonds. It should be noted that this analysis is essentially unchanged when density functional therory orbitals are utilized.

Analysis of the actinyl T-shaped dimers reveals significant charge transfer between monomers.   For all dimers examined here, an O atom of the electron donor unit coordinates the An center of the electron acceptor.   The donor is slightly electron deficient at all geometries, relative to the integer charges of the separated monomers.   Figure 5 shows the geometry dependence of the charge transfer in the dimers, as measured by the excess positive charge of the donor (equivalent to the fractional number of electrons transferred to the acceptor).   At equilibrium geometries (R=0) several hundredths of an electron are transferred from the O atom of the donor to the An center of the acceptor.   Perturbative analysis of the Fock matrix shows that charge transfer originates predominantly from the σ-type O lone pair of the donor as density delocalizes into vacant valence An hybrids (of mixed 7s, 6d, and 5f character) of the acceptor. There is no evidence in this analysis of any significant π-type charge transfer, either to or from the acceptor.   Figure 6 shows the geometry dependence of the second-order interaction energies for σ-type charge transfer in the dimers.   Charge transfer diminishes rapidly as the monomers are separated and donor-acceptor orbital overlap weakens.   From Figures 5 and 6 we see that the $(UO_2^{2+})(UO_2^+)$ heterodimer exhibits the strongest interaction, transferring 0.112 electrons from the UO_2^+ donor to the UO_2^{2+} acceptor at the equilibrium geometry and stabilizing the dimer by 30.7 kcal/mol.   We note that the strength of the charge transfer interaction at the equilibrium geometry (from Figure 6) is at least double the dissociation barrier height (from Table IV) for every actinyl dimer examined here.   This suggests that charge transfer is largely responsible for the stability of the CCI complexes.

The extent of charge transfer depends most strongly on the identity of the donor, with donor strength decreasing for the series $UO_2^+ > NpO_2^+ > PuO_2^+ > AmO_2^+$.   This trend likely stems

from the increasing s-character of the donor O lone pair, from 84% s-character in UO_2^+ to 88% s

in AmO_2^+ (Table V).   In accord with Bent's Rule ,[55] the increasing electronegativity of the An

center from U to Am, as reflected in the decreasing polarities of the σ_{AnO} bond (see the bond

ionicities of Table V), draws p_z-character at the O atom into the bond and leaves the lone pair

increasingly s-rich.   The elevated s-character stabilizes the lone pair, decreasing its tendency to

donate electrons compared to lone pairs of higher p-character.   Thus, the s-rich lone pair of

AmO_2^+ is a weaker donor than the lone pair of UO_2^+.   NBO analysis also reveals why An(VI)

monomers (AnO_2^{2+}) are more effective acceptors than An(V) monomers (AnO_2^+).   The extra

5f electron in an An(V) acceptor raises the energies of its vacant valence orbitals, diminishing

the tendency of these orbitals to accept electrons from a donor monomer.

   The picture of charge transfer in the T-shaped actinyl dimers that emerges from NBO

analysis differs significantly from that described by McKee and Swart[11] based on an atomic

multipole expansion of the electron density.   The multipole expansion suggests that π-type

interactions dominate charge transfer, specifically $5f_\pi \rightarrow \pi_{AnO}^*$ back-bonding interactions in

$(NpO_2^+)(NpO_2^+)$ and $(NpO_2^{2+})(UO_2^+)$ and $\pi_{AnO} \rightarrow 5f_\pi$ forward-bonding interactions in

$(UO_2^{2+})(NpO_2^+)$.   The donor/acceptor roles of the monomers in this description thus depend on

the identities and oxidation states of the An centers.   In contrast, NBO analysis reveals no

significant π-type interactions and that the electron donor always coordinates the acceptor at the

An center.   That the NBO and multipole expansion pictures differ is not particularly surprising

considering that the two are distinctly different approaches to analyzing the electron density.

The NBO method has the advantage that it directly calculates a numerically stable, orbital-based

representation of the density, including orbital occupancies and perturbative interaction strengths.

One can generally only speculate what roles the orbitals play from an analysis of atomic charges

from the multipole expansion.

   We also examined charge transfer in the $(UO_2^+)(UO_2^+)$ side-on dimer, which is stronger

than that of any of the T-shaped dimers.   In the equilibrium side-on geometry an in-plane π_{UO}

bond and O lone pair of one monomer overlap a valence U acceptor orbital of approximate s^2d^2f

character of the second monomer.   The bond and lone pair together transfer 0.043 electrons to

the acceptor.   The C_{2h} symmetry of the dimer likewise requires that a bond and lone pair of the second monomer back-donate 0.043 electrons to an acceptor orbital of the first.   These four orbital interactions collectively stabilize the side-on dimer geometry by 47.1 kcal/mol, which is over 50% stronger than the strongest charge transfer interaction exhibited by any of the T-shaped dimers.

It might be noted at this point that the stability trend of the T-shaped CCI dimers can be qualitatively reproduced by inspection of the atomic charges on the monomer units, i.e., using the natural population analysis (NPA) charges of Vasiliu et al,[56] the current values in Table V, or the experimentally derived charges for U(VI) of Choppin and Rao.[57] These trends, however, generally just reflect the differences in the actinide electronegativities (relative to that of oxygen). Correlation of these trends with dimer dissociation energies (or other properties of the dimers) may be largely fortuituous. What NBO analysis offers, beyond NPA, is a more detailed description of the orbital interactions and electron transfers in the dimers that are entirely consistent with the NPA charges of the monomers in the dimer complexes (as shown in Fig. 5).

IV. CONCLUSIONS

A variety of actinyl dimer systems involving both Actinyl(VI) and Actinyl(V) cations have been studied using composite coupled cluster methods for the first time with correlation consistent basis sets and extrapolation to the CBS limit. While all of the cation-cation dimers studied are thermodynamically unstable due to Coulombic repulsion, many were calculated to be metastable. Nearly all of the species studied in this work involved T-shaped molecular geometries, whereby an oxo-group of a donor actinyl transfers electrons to the actinide center of an acceptor actinyl. The most stable dimers are predicted to occur when the acceptor has a +2 charge, i.e., an An(VI) actinyl, and the donor has a +1 charge, i.e., an An(V) actinyl. Local minima were not found when both the acceptor and donor involved an An(VI) actinyl. In particular, the stability of the mixed valent dimers was nearly totally dependent on the identity of the An(V) donor actinyl and more open-shell electrons decreased the stability. For An(V) homodimers, the stability also decreased with an increase in the number of open-shell electrons, i.e., U(V) > Np(V) > Pu(V) > Am(V). These trends were rationalized by extensive natural bond orbital analyses, including those for the isolated monomers, which indicated the stability of a CCI complex is largely determined by charge transfer from the σ-type O lone pair of the donor

15

to empty valence An hybrid orbitals of the acceptor. Significant π-type charge transfer was not found. The decreasing donor strength from UO_2^+ to AmO_2^+ correlates with the increase in s-character of the donor O lone pair. Somewhat surprisingly, the $6p_z$ of the An significantly contribute to the σ-type bonds in the monomers.

The results of the present calculations agree qualitatively with previous experimental investigations in condensed phases, e.g., it is very uncommon to observe a U(VI) -–U(VI) CCI in any uranyl crystal structures,[22] which correlates with the lack of a calculated local minimum for the $(UO_2^{2+})(UO_2^{2+})$ dimer in the gas phase. There has not been much experimental work published for CCIs involving trans-neptunium actinyls, but empirical stability arguments[8] agree well with the results of this work, i.e., the stability of An(V) CCI complexes decreases in the donor series $UO_2^+>NpO_2^+>PuO_2^+>AmO_2^+$ and the activity of AnO_2^{2+} as an acceptor in CCI complexes decreases with the same periodic trend $UO_2^{2+}>NpO_2^{2+}>PuO_2^{2+}>AmO_2^{2+}$. The present work indicates that at least for U(VI) and Np(VI), this last trend is only very weakly obeyed.

Most CCI side-on dimers were found to exhibit strong multi-reference character, hence only the side-on dimer $UO_2^+UO_2^+$ was studied in this work since the CCSD(T) method was found to be reliable in this case. It was calculated to be thermodynamically more stable than the analogous T-shaped dimer by nearly 10 kcal/mol.

SUPPLEMENTAL MATERIAL

See supplemental material for Tables S1-S4 containing equilibrium geometries and harmonic frequencies for the monomer unit, equilibrium geometries and harmonic frequencies for the dimers, and the cartesian coordinates for the calculatd minimum energies paths for formation of the T-shaped dimers.

CONFLICTS OF INTEREST

There are no conflicts of interest to declare.

ACKNOWLEDGDEMENTS

REFERENCES

1. J. B. Goodenough, *Phys. Rev. A*, 1960, **117**, 1442-1451.

2. P. M. Almond, S. Skanthakumar, L. Soderholm and P. C. Burns, *Chem Mater*, 2007, **19**, 280-285.

3. J. C. Sullivan, J. C. Hindman and A. J. Zielen, *J. Am. Chem. Soc*, 1961, **83**, 3373-3378.

4. B. Guillaume, G. M. Begun and R. L. Hahn, *Inorg Chem*, 1982, **21**, 1159-1166.

5. V. A. M. Vodovatov, L.G.; Suglobov, D.N., *Radiokhimiya*, 1979, **21**, 830-835.

6. V. A. K. Vodovatov, V.B.; Kovaleva, T.V.; Mashirov, L.G.; Suglobov, D.N.; Sles, V.G., *Radiokhimiya*, 1975, **17**, 889.

7. S. Skanthakumar, M. R. Antonio and L. Soderholm, *Inorg Chem*, 2008, **47**, 4591-4595.

8. N. N. Krot and M. S. Grigoriev, *Russ. Chem. Rev.*, 2004, **73**, 89-100.

9. V. N. S. Serezhkin, G. V.; Pushkin, D. V.; Serezhkina, L. B., *Radiochem.*, 2014, **56**, 115-133.

10. M. B. Andrews and C. L. Cahill, *Chem. Rev.*, 2013, **113**, 1121-1136.

11. M. L. McKee and M. Swart, *Inorg Chem*, 2005, **44**, 6975-6982.

12. B. Vlaisavljevich, P. Miro, D. X. Ma, G. E. Sigmon, P. C. Burns, C. J. Cramer and L. Gagliardi, *Chem Eur J*, 2013, **19**, 2937-2941.

13. A. Ekstrom, *Inorg. Chem.*, 2002, **13**, 2237-2241.

14. H. Steele and R. J. Taylor, *Inorg Chem*, 2007, **46**, 6311-6318.

15. G. B. Jin, S. Skanthakumar and L. Soderholm, *Inorg Chem*, 2012, **51**, 3220-3230.

16. G. B. Jin, *Inorg Chem*, 2016, **55**, 2612-2619.

17. G. B. Jin, S. Skanthakumar and L. Soderholm, *Inorg Chem*, 2011, **50**, 5203-5214.

18. S. Wang, J. Diwu, E. V. Alekseev, L. J. Jouffret, W. Depmeier and T. E. Albrecht-Schmitt, *Inorg Chem*, 2012, **51**, 7016-7018.

19. T. Z. Forbes and P. C. Burns, *J Solid State Chem*, 2007, **180**, 106-112.

20. T. Z. Forbes and P. C. Burns, *Inorg Chem*, 2008, **47**, 705-712.

21. T. Z. Forbes and P. C. Burns, *J Solid State Chem*, 2009, **182**, 43-48.

22. B. Xiao, H. Schlenz, J. Dellen, D. Bosbach, E. V. Suleimanov and E. V. Alekseev, *Cryst Growth Des*, 2015, **15**, 3775-3784.

23. E. V. Alekseev, S. V. Krivovichev, T. Malcherek and W. Depmeier, *Inorg Chem*, 2007, **46**, 8442-8444.

24. E. Balboni and P. C. Burns, *J Solid State Chem*, 2014, **213**, 1-8.

25. D. Schröder and H. Schwarz, *J Phys Chem A*, 1999, **103**, 7385-7394.

26. P. Tecmer, S. W. Hong and K. Boguslawski, *Phys Chem Chem Phys*, 2016, **18**, 18305-18311.

27. P. J. Knowles, C. Hampel and H.-J. Werner, *J Chem Phys*, 1993, **99**, 5219-5227.

28. K. Raghavachari, G. W. Trucks, J. A. Pople and M. Head-Gordon, *Chem. Phys. Lett.*, 1989, **157**, 479-483.

29. J. D. Watts, J. Gauss and R. J. Bartlett, *J. Chem. Phys.*, 1993, **98**, 8718-8733.

30. M. Douglas and N. M. Kroll, *Ann. Phys.*, 1974, **82**, 89-155.

31. G. Jansen and B. A. Hess, *Phys. Rev. A*, 1989, **39**, 6016.

32. M. Reiher and A. Wolf, *J Chem Phys*, 2004, **121**, 10945-10956.

33. R. Feng and K. A. Peterson, *J Chem Phys*, 2017, **147**, 084108-084112.

34. T. H. Dunning Jr, *J. Chem. Phys.*, 1989, **90**, 1007.

35. R. A. Kendall, T. H. Dunning, Jr. and R. J. Harrison, *J Chem Phys*, 1992, **96**, 6796-6806.

36. W. A. de Jong, R. J. Harrison and D. A. Dixon, *J Chem Phys*, 2001, **114**, 48-53.

37. I. Infante, A. Kovacs, G. La Macchia, A. R. M. Shahi, J. K. Gibson and L. Gagliardi, *J Phys Chem A*, 2010, **114**, 6007-6015.

38. D. Feller, K. A. Peterson and D. A. Dixon, *J Chem Phys*, 2008, **129**, 204105.

39. K. A. Peterson, D. Feller and D. A. Dixon, *Theor Chem Acc*, 2012, **131**, 1079.

40. D. A. Dixon, D. Feller and K. A. Peterson, *Ann Rep Comp Chem*, 2012, **8**, 1-28.

41. A. Karton and J. M. L. Martin, *J Chem Phys*, 2006, **125**.

42. J. M. L. Martin, *Chem. Phys. Lett.*, 1996, **259**, 669-678.

43. D. Feller, K. A. Peterson and J. G. Hill, *J Chem Phys*, 2011, **135**.

44. O. Visser, L. Visscher, P. J. C. Aerts and W. C. Nieuwpoort, *J Chem Phys*, 1992, **96**, 2910-2919.

45. K. G. Dyall, *J Chem Phys*, 1994, **100**, 2118-2127.

46. L. Visscher and K. G. Dyall, *Atomic Data and Nuclear Data Tables*, 1997, **67**, 207-224.

47. H. J. Werner, P. J. Knowles, G. Knizia, F. R. Manby and M. Schutz, *Wires Comput Mol Sci*, 2012, **2**, 242-253.

48. MOLPRO is a package of ab initio programs written by H.-J. Werner, P. J. Knowles, G. Knizia, F. R. Manby, M. Schütz, P. Celani, W. Györffy, D. Kats, T. Korona, R. Lindh, A. Mitrushenkov, G. Rauhut, K. R. Shamasundar, T. B. Adler, R. D. Amos, A. Bernhardsson, A. Berning, D. L. Cooper, M. J. O. Deegan, A. J. Dobbyn, F. Eckert, E. Goll, C. Hampel, A.

Hesselmann, G. Hetzer, T. Hrenar, G. Jansen, C. Köppl, Y. Liu, A. W. Lloyd, R. A. Mata, A. J. May, S. J. McNicholas, W. Meyer, M. E. Mura, A. Nicklaß, D. P. O'Neill, P. Palmieri, D. Peng, K. Pflüger, R. Pitzer, M. Reiher, T. Shiozaki, H. Stoll, A. J. Stone, R. Tarroni, T. Thorsteinsson, M. Wang .

49. CFOUR, Coupled-Cluster techniques for Computational Chemistry, a quantum-chemical program package by J.F. Stanton, J. Gauss, L. Cheng, M.E. Harding, D.A. Matthews, P.G. Szalay with contributions from A.A. Auer, R.J. Bartlett, U. Benedikt, C. Berger, D.E. Bernholdt, Y.J. Bomble, O. Christiansen, F. Engel, R. Faber, M. Heckert, O. Heun, M. Hilgenberg, C. Huber, T.-C. Jagau, D. Jonsson, J. Jusélius, T. Kirsch, K. Klein, W.J. Lauderdale, F. Lipparini, T. Metzroth, L.A. Mück, D.P. O'Neill, D.R. Price, E. Prochnow, C. Puzzarini, K. Ruud, F. Schiffmann, W. Schwalbach, C. Simmons, S. Stopkowicz, A. Tajti, J. Vázquez, F. Wang, J.D. Watts and the integral packages MOLECULE (J. Almlöf and P.R. Taylor), PROPS (P.R. Taylor), ABACUS (T. Helgaker, H.J. Aa. Jensen, P. Jørgensen, and J. Olsen), and ECP routines by A. V. Mitin and C. van Wüllen. For the current version, see http://www.cfour.de.

50. DIRAC, a relativistic ab initio electronic structure program, Release DIRAC17 (2017), written by L. Visscher, H. J. Aa. Jensen, R. Bast, and T. Saue, with contributions from V. Bakken, K. G. Dyall, S. Dubillard, U. Ekström, E. Eliav, T. Enevoldsen, E. Faßhauer, T. Fleig, O. Fossgaard, A. S. P. Gomes, E. D. Hedegård, T. Helgaker, J. Henriksson, M. Iliaš, Ch. R. Jacob, S. Knecht, S. Komorovský, O. Kullie, J. K. Lærdahl, C. V. Larsen, Y. S. Lee, H. S. Nataraj, M. K. Nayak, P. Norman, G. Olejniczak, J. Olsen, J. M. H. Olsen, Y. C. Park, J. K. Pedersen, M. Pernpointner, R. Di Remigio, K. Ruud, P. Sałek, B. Schimmelpfennig, A. Shee, J. Sikkema, A. J. Thorvaldsen, J. Thyssen, J. van Stralen, S. Villaume, O. Visser, T. Winther, and S. Yamamoto (see http://www.diracprogram.org).

51. F. Weinhold and C. L. Landis, *Valency and Bonding: A Natural Donor-Acceptor Perspective*, Cambridge University Press, 2005.

52. NBO 7.0.   E. D. Glendening, J. K. Badenhoop, A. E. Reed, J. E. Carpenter, J. A. Bohmann, C. M. Morales, P. Karafiloglou, C. R. Landis, and F. Weinhold, Theoretical Chemistry Institute, University of Wisconsin, Madison, WI (2018)

53. J. Marçalo and J. K. Gibson, *J. Phys. Chem. A*, 2009, **113**, 12599-12606.

54. R. J. Baker, *Chem Eur J*, 2012, **18**, 16258-16271.

55. H. A. Bent, *Chem. Rev.*, 1961, **61**, 275-311.

56. M. Vasiliu, J. K. Gibson, K. A. Peterson and D. A. Dixon, *Chem Eur J*, 2019, **17**, 602-611.

57. G. R. Choppin and L. F. Rao, *Radiochim. Acta*, 1984, **37**, 143-146.

Physical Chemistry Chemical Physics

Page 22 of 34

Table I. Ground-state electronic configurations and equilibrium bond lengths of actinyl monomers obtained at the DKH3-CCSD(T)/VTZ level of theory.

Actinyl cation	State	Open-shell Composition	Bond length, Å
UO_2^{2+}	$^1\Sigma_g^+$	---	1.700
UO_2^+	$^2\Phi_u$	$(5f_\phi)^1$	1.760
NpO_2^{3+}	$^1\Sigma_g^+$	---	1.675
NpO_2^{2+}	$^2\Phi_u$	$(5f_\phi)^1$	1.694
NpO_2^+	^3H_g	$(5f_\phi)^1(5f_\delta)^1$	1.737
PuO_2^{3+}	$^2\Phi_u$	$(5f_\phi)^1$	1.684
PuO_2^{2+}	^3H_g	$(5f_\phi)^1(5f_\delta)^1$	1.681
PuO_2^+	$^4\Phi_u$	$(5f_\phi)^1(5f_\delta)^2$	1.719
AmO_2^{3+}	^3H_g	$(5f_\phi)^1(5f_\delta)^1$	1.683
AmO_2^{2+}	$^4\Phi_u$	$(5f_\phi)^1(5f_\delta)^2$	1.671
AmO_2^+	$^5\Sigma_g^+$	$(5f_\phi)^2(5f_\delta)^2$	1.720

22

Table II. T-shaped dimer systems that were investigated at the CCSD(T) level of theory. "A" = acceptor, "D" = donor. "✓" denotes that a local minimum was found, "✗" a local minimum was not found, "–" the dimer combination was not tested.

A \ D	UO_2^{2+}	UO_2^{+}	NpO_2^{3+}	NpO_2^{2+}	NpO_2^{+}	PuO_2^{3+}	PuO_2^{2+}	PuO_2^{+}	AmO_2^{3+}	AmO_2^{2+}	AmO_2^{+}
UO_2^{2+}	✗	✓	✗	✗	✓	✗ [a]	–	–	–	–	–
UO_2^{+}	✗	✓	✗ [a]	✗	–	–	–	–	–	–	–
NpO_2^{3+}	✗	✗ [a]	✗	✗	–	–	–	–	–	–	–
NpO_2^{2+}	✗	✓	✗	✗	✓	–	–	–	–	–	–
NpO_2^{+}	–	–	✗	✗	✓	–	–	–	–	–	–
PuO_2^{3+}	–	✗ [a]	–	–	–	✗	✗	–	–	–	–
PuO_2^{2+}	–	✓	–	–	–	✗	✗	–	–	–	–
PuO_2^{+}	–	–	–	–	–	✗	–	✓	–	–	–
AmO_2^{3+}	–	–	–	–	–	–	–	–	✗	–	–
AmO_2^{2+}	–	✓	–	–	–	–	–	–	–	✗	–
AmO_2^{+}	–	–	–	–	–	–	–	–	–	–	✓

[a] Too multireference for CCSD(T) due to the large charge transfer from the +3 monomer to the +1 fragment. They are expected to be unstable, however, due to comparison to the analogous +2/+2 cases.

Table III. CCSD(T) composite results[a] for 0 K CCI dissociation energies (kcal/mol).

Acceptor:	UO_2^{2+}	UO_2^{2+}	NpO_2^{2+}	UO_2^+	NpO_2^+	PuO_2^+	AmO_2^+	Side-on
Donor:	UO_2^+	NpO_2^+	UO_2^+	UO_2^+	NpO_2^+	PuO_2^+	AmO_2^+	$UO_2^+UO_2^+$
E_{VQZ}[b]	-83.36	-87.80	-88.26	-48.16	-59.26	-52.49	-54.34	-38.45
$\Delta CBS[TQ]$[c]	-0.28	-0.34	-0.23	-0.21	-0.23	-0.25	-0.29	-0.16
ΔSO	-0.16	-2.38	-0.31	-1.06	-4.71	-3.91	-3.41	+0.24
$\Delta Gaunt$	-1.31	-1.60	-0.78	-0.46	-0.33	-0.23	+0.17	-1.20
ΔZPE	-0.45	-0.59	-0.76	-0.26	-0.38	-0.18	-0.20	-0.96
$E_{diss,FPD}$	-85.56	-92.71	-90.34	-50.16	-64.91	-57.07	-58.06	-40.28

[a] See Eq. (1).

[b] DKH3-CCSD(T)/cc-pVQZ-DK3(An)/aug-cc-pVQZ-DK(O)

[c] CBS limits obtained from application of Eqs. (2) and (3). See the text.

Table IV. Composite results[a] for T-shaped CCI barrier heights (kcal/mol) and the corresponding CCSD(T)/VTZ CCI equilibrium and transition state dimer separations, as well as the geometry changes relative to separated monomers upon complexation (Å and degrees).[b]

Acceptor:	UO_2^{2+}	UO_2^{2+}	NpO_2^{2+}	NpO_2^{2+}	UO_2^+	NpO_2^+	PuO_2^+	AmO_2^+
Donor:	UO_2^+	NpO_2^+	UO_2^+	NpO_2^+	UO_2^+	NpO_2^+	PuO_2^+	AmO_2^+
E_{VQZ}^c	14.74	11.83	14.80	11.93	6.05	1.59	0.58	0.03
$\Delta CBS[TQ]^d$	0.09	0.06	0.09	0.06	0.62	-0.04	-0.01	-0.01
ΔSO	+1.10	+0.39	+0.58	-1.91	+0.17	-0.11	+0.61	-0.12
$\Delta Gaunt$	-0.72	-0.26	-0.48	1.52	-1.29	-0.20	-0.35	-0.05
$E_{b,FPD}$	15.21	12.02	14.99	11.60	5.56[e]	1.23	0.82	-0.15
R_b^{CCI}	3.845	3.769	3.829	3.750	3.720	3.525	3.291	3.083
R_e^{CCI}	2.445	2.469	2.429	2.450	2.720	2.725	2.791	2.883
Δr_a	+0.010	+0.009	-0.003	-0.004	+0.007	-0.006	+0.004	+0.003
Δr_{d1}	+0.146	+0.137	+0.145	+0.137	+0.060	+0.057	+0.051	+0.046
Δr_{d2}	-0.033	-0.028	-0.033	-0.028	-0.019	-0.016	-0.014	-0.012
$\Delta \theta_a$	+0.03	-0.12	-0.28	---	-5.68	-2.13	-1.69	---

[a] See Eq. (1).

[b] Negative values of Δr indicate the bond length shortened upon complexation. $\Delta \theta_a$ is the change in the acceptor O-An-O angle; a negative value indicates the acceptor molecule is bending towards the donor.   See Fig. 1 for coordinate defintions.

[c] DKH3-CCSD(T)/cc-pVQZ-DK3(An)/aug-cc-pVQZ-DK(O)

[d] CBS limits obtained from application of Eqs. (2) and (3). See the text.

[e] Note that the metastable minimum of the side-on dimer is lower in energy than the T-shaped isomer by 9.89 kcal/mol.   See Table III.

Table V. NPA charges and Lewis orbitals, including orbital type, occupancy, ionicity, and hybrid character by atomic center for the actinyl monomers.[a]

monomer	$q(An/O)$	type	occupancy	percent ionicity[b]	center	hybrid character[c]			
						%s	%p	%d	%f
UO_2^{2+}	+3.14/-0.57	n_O	1.979		O	85	15	0	0
		σ_{UO}	1.946	38.0	U	2	17	48	33
					O	15	85	1	0
		π_{UO}	1.997	61.7	U	0	1	50	49
					O	0	100	0	0
NpO_2^{2+}	+3.01/-0.51	n_O	1.979		O	84	16	0	0
		σ_{NpO}	1.928	33.9	Np	2	18	48	32
					O	14	86	1	0
		π_{NpO}	1.995	60.7	Np	0	1	50	49
					O	0	100	0	0
UO_2^{+}	+2.69/-0.85	n_O	1.979		O	84	16	0	0
		σ_{UO}	1.957	46.4	U	2	12	47	38
					O	16	83	1	0
		π_{UO}	2.000	71.0	U	0	0	50	50
					O	0	100	0	0
NpO_2^{+}	+2.59/-0.80	n_O	1.978		O	85	15	0	0
		σ_{NpO}	1.943	42.2	Np	2	14	47	36
					O	15	84	1	0
		π_{NpO}	2.000	71.1	Np	0	0	50	50
					O	0	100	0	0
PuO_2^{+}	+2.51/-0.76	n_O	1.978		O	86	14	0	0
		σ_{PuO}	1.929	38.4	Pu	2	16	47	34
					O	14	85	1	0
		π_{PuO}	2.000	70.9	Pu	0	0	50	50
					O	0	100	0	0
AmO_2^{+}	+2.47/-0.73	n_O	1.977		O	89	11	0	0
		σ_{AmO}	1.908	34.3	Pu	2	17	48	33
					O	11	88	1	0
		π_{AmO}	2.000	72.0	Pu	0	0	50	50
					O	0	100	0	0

[a] Charges and NBOs calculated at the HF level.

[b] The ionicity for normalized NBO $\Omega_{AB} = c_A h_A + c_B h_B$ of hybrid orbitals h_A, h_B is $c_B{}^2 - c_A{}^2$.

[c] Percentages refer to the 2s and 2p on O, 7s, 6p, 6d, and 5f on An.

Figure 1. T-shaped and side-on CCl dimers.
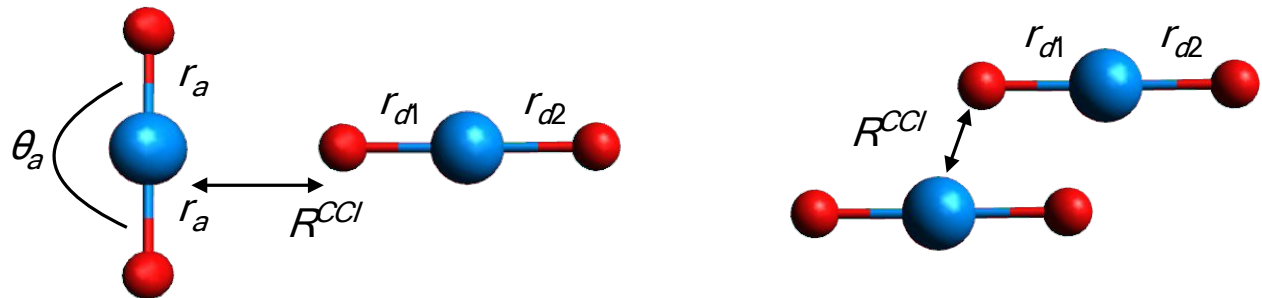
Figure 2. Calculated 1-D potential energy curve at the CCSD(T)/VTZ level of theory for the T-shaped dimer $(UO_2^{2+})(NpO_2^+)$. R_e^{CCl} is the equilibrium bond length of the local minimum; R_b^{CCl} is the bond length of the structure at the top of the barrier.
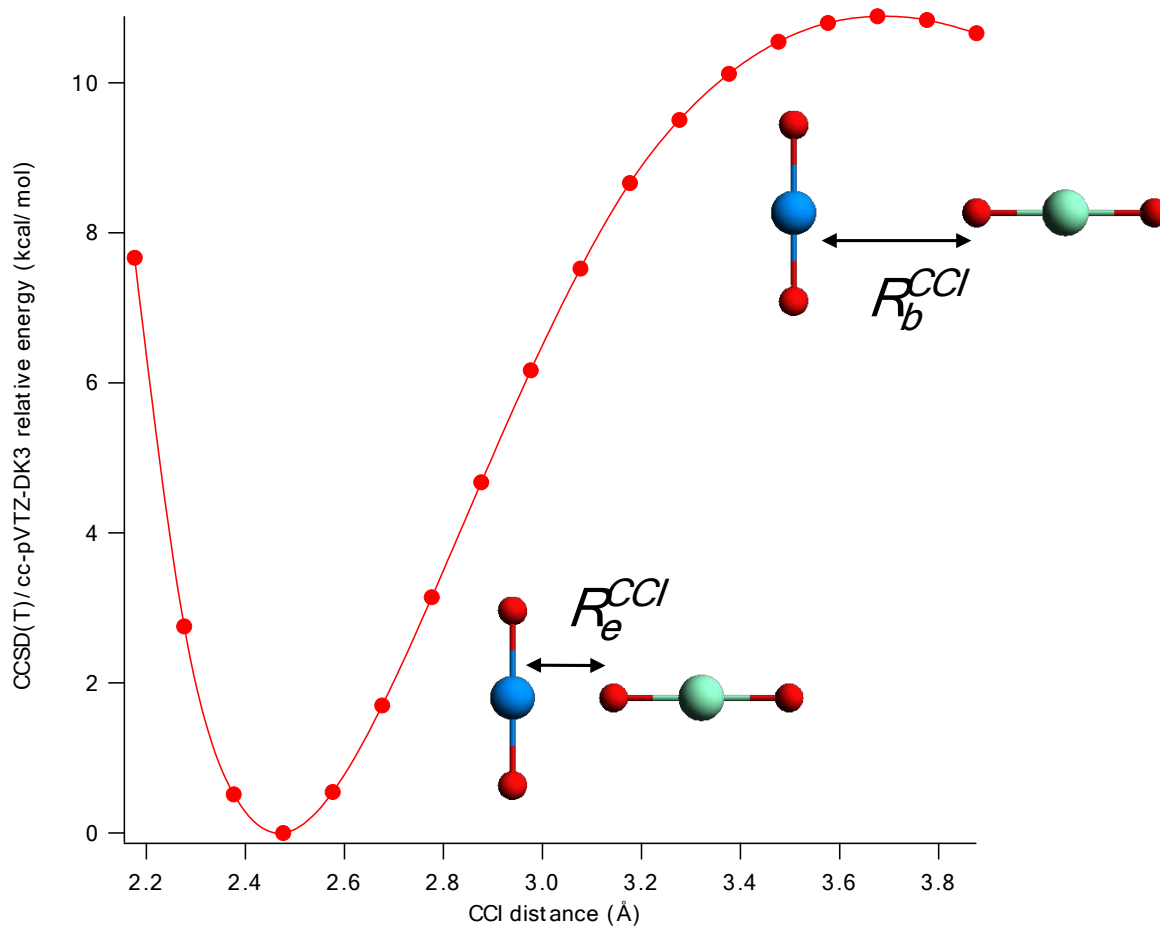
Figure 3. Calculated 1-D potential energy curves at the CCSD(T)/VTZ level of theory for the T-shaped heterodimers $UO_2^{2+}NpO_2^+$, $NpO_2^{2+}NpO_2^+$, $UO_2^{2+}NpO_2^+$, $NpO_2^{2+}UO_2^+$.
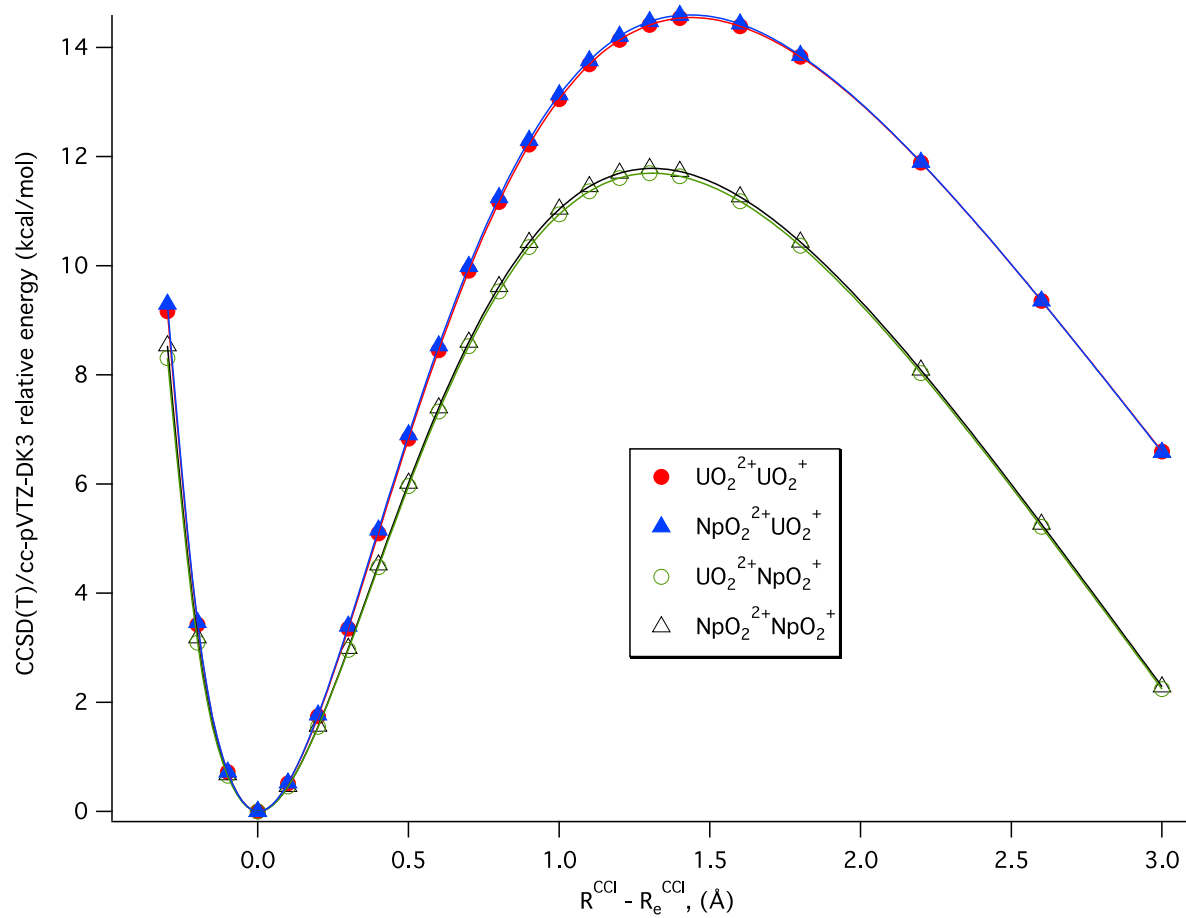
Figure 4. Calculated 1-D potential energy curves at the CCSD(T)/VTZ level of theory for the T-shaped homodimers $UO_2^+UO_2^+$, $NpO_2^+NpO_2^+$, $PuO_2^+PuO_2^+$, $AmO_2^+AmO_2^+$.
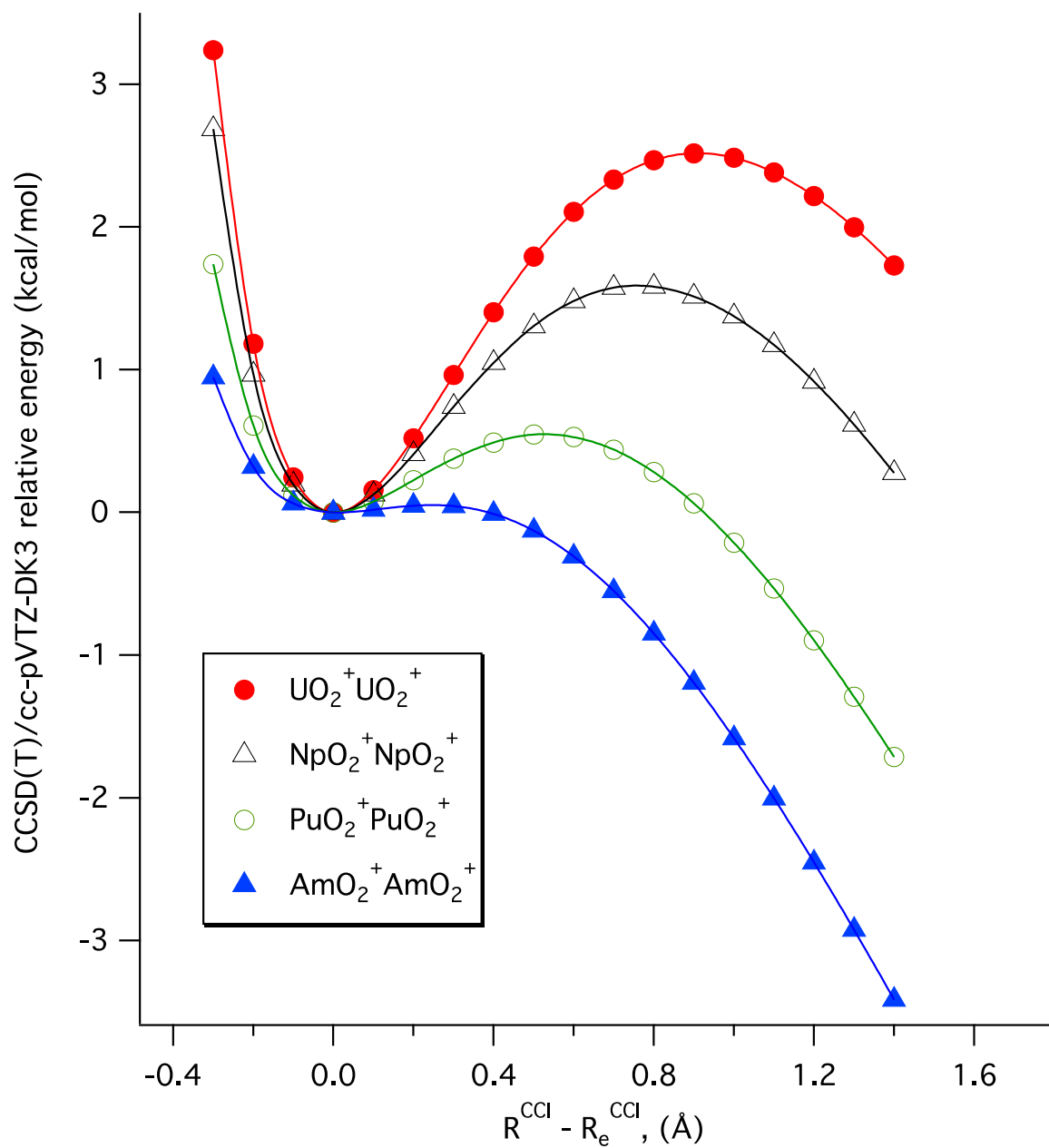
Figure 5.   Electron density transferred from donor to acceptor in the (a) T-shaped heterodimers and (b) T-shaped homodimers, as a function of monomer separation relative to the equilibrium geometries of the dimers

(a)   (b)
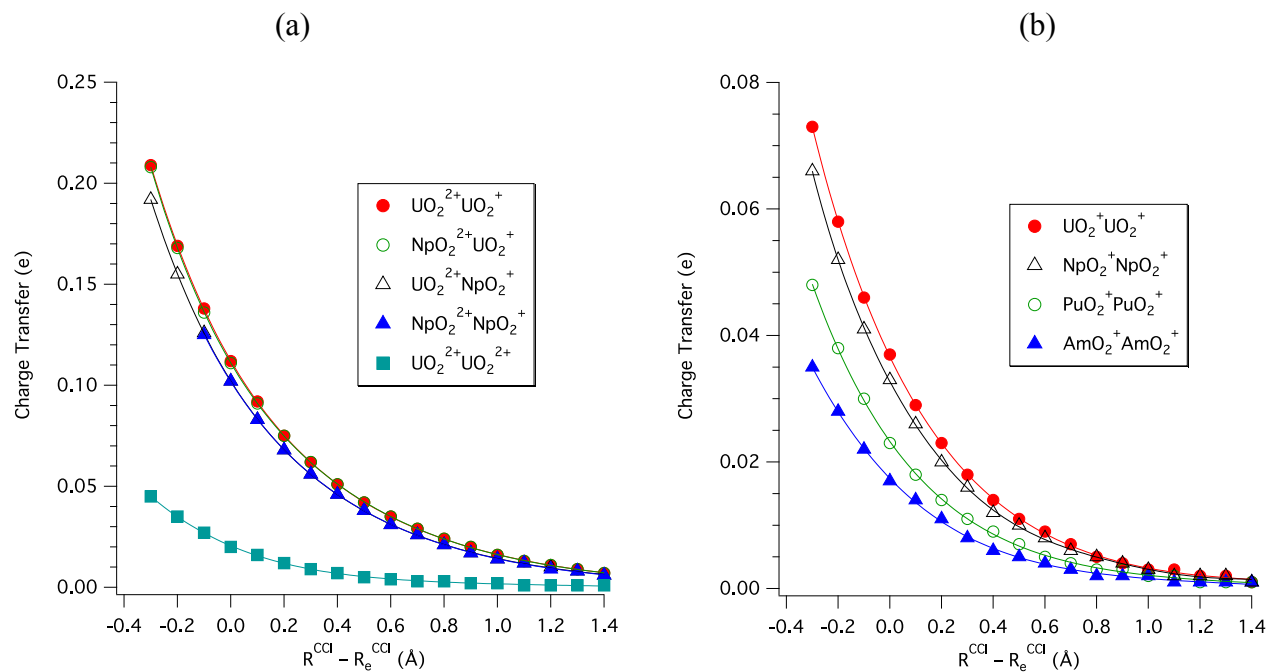
Figure 6.   Strengths of the charge transfer interactions in the (a) T-shaped heterodimers and (b) T-shaped homodimers, as a function of monomer separation relative to the equilibrium geometries of the dimers.

(a)   (b)
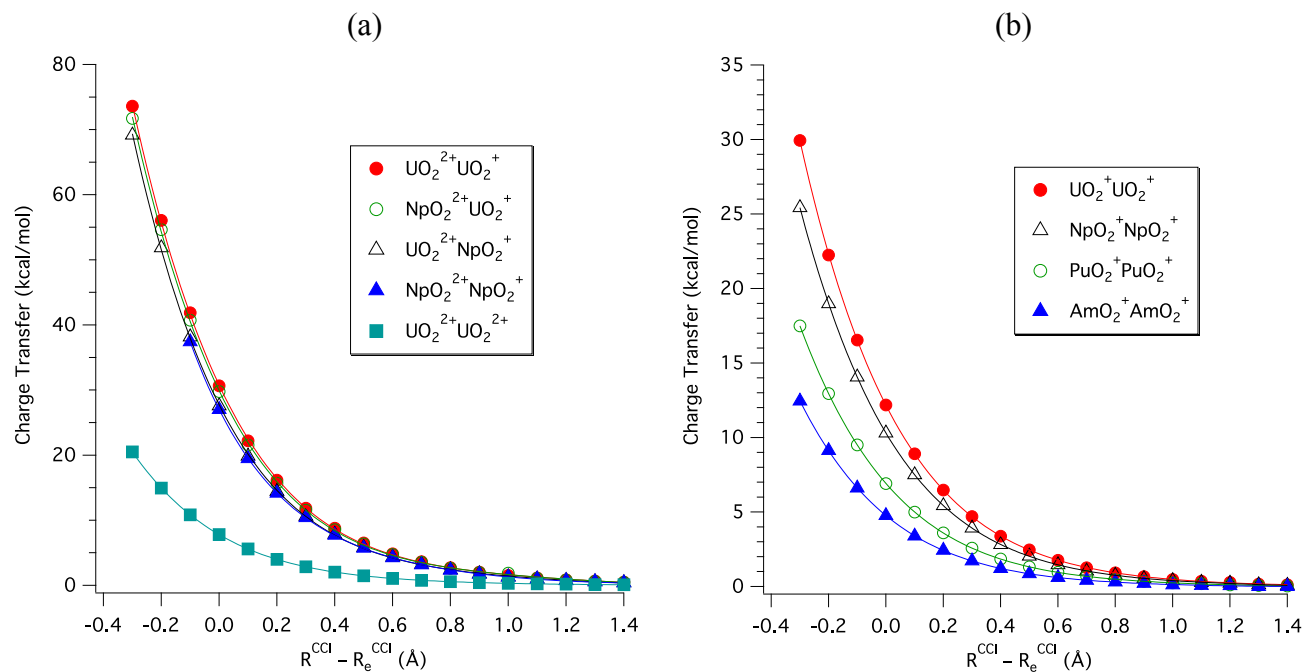
Accurate coupled cluster calculations of actinyl cation-cation interactions suggest significant gas phase kinetic stabilities that correlate well with known species in condensed phases